Computational Investigation of a Boundary-Layer Ingesting Propulsion System for the Common Research Model

Brennan T. Blumenthal[1]
NASA Johnson Space Center, Houston, TX 77058

Alaa A. Elmiligui[2], Karl A. Geiselhart[3], Richard L. Campbell[4]
NASA Langley Research Center, Hampton, VA 23681

Mark D. Maughmer[5], Sven Schmitz[6]
Pennsylvania State University, University Park, PA 16802

The present paper examines potential propulsive and aerodynamic benefits of integrating a Boundary-Layer Ingestion (BLI) propulsion system into the Common Research Model (CRM) geometry and the NASA Tetrahedral Unstructured Software System (TetrUSS). The Numerical Propulsion System Simulation (NPSS) environment is used to generate engine conditions for Computational Fluid Dynamics (CFD) analyses. Improvements to the BLI geometry are made using the Constrained Direct Iterative Surface Curvature (CDISC) design method. Potential benefits of the BLI system relating to cruise propulsive power are quantified using a power balance method, and a comparison to the baseline case is made. Iterations of the BLI geometric design are shown, and improvements between subsequent BLI designs are presented. Simulations are conducted for a cruise flight condition of Mach 0.85 at an altitude of 38,500 feet, with Reynolds number of 40 million based on mean aerodynamic chord and an angle of attack of 2° for all geometries. Results indicate an 8% reduction in engine power requirements at cruise for the BLI configuration compared to the baseline geometry. Small geometric alterations of the aft portion of the fuselage using CDISC has been shown to marginally increase the benefit from boundary-layer ingestion further, resulting in an 8.7% reduction in power requirements for cruise, as well as a drag reduction of approximately twelve counts over the baseline geometry.

Nomenclature

A_j	Jet exit area, ft^2	p_{0jet}	Total pressure of jet
AR	Aspect Ratio	q_∞	Free-stream dynamic pressure, Pa
C_D	Drag coefficient	Re	Reynolds number based on mean aerodynamic chord
C_L	Lift coefficient	S_{ref}	Geometry reference area, in^2
C_{Pk}	Net propulsor power coefficient	T	Thrust, lb_f
C_p	Pressure coefficient	U	Potential energy, $ft\text{-}\ lb_f$
C_{ref}	Chord reference length	u	Flow velocity, ft/s
C_T	Thrust coefficient	u_j	Engine exit velocity, ft/s
C_X	Net streamwise force coefficient in the x-axis	u_j'	Engine exit velocity, BLI propulsor, ft/s
D	Drag force, lb_f	u_j''	Flow velocity at BLI propulsor exit
D_A	Drag due to airframe, lb_f	u_w	Flow velocity of ingested wake, ft/s
F_x	Net streamwise force, lb_f	u_∞	Free-stream velocity, ft/s
J	Advance ratio	V	Velocity magnitude, ft/s
K	Kinetic energy, $ft\text{-}\ lb_f$	X_{ref}	Moment center in X-direction
M	Mach number	Y_{ref}	Moment center in Y-direction
$\dot{m}$	Mass flow rate, $slug/s$	Z_{ref}	Moment center in Z-direction
P	Power, lb_f/s	α	Angle of attack, °
P_k	Net mechanical power, propulsor faces, lb_f/s	Δ	Change in quantity
P_s	Shaft power, moving surfaces, lb_f/s	δ	Boundary-layer thickness, $inch$

[1] Flight Dynamics Officer, Flight Dynamics and Operations Branch, AIAA Member.
[2] Aerospace Engineer, Configuration Aerodynamics Branch, Mail Stop 499, AIAA Senior Member.
[3] Aerospace Engineer, Aeronautics Systems Analysis Branch, Mail Stop 422, AIAA Associate Fellow.
[4] Aerospace Engineer, Configuration Aerodynamics Branch, Mail Stop 499, AIAA Member.
[5] Professor, Department of Aerospace Engineering, AIAA Associate Fellow.
[6] Associate Professor, Department of Aerospace Engineering, AIAA Senior Member.

P_v	Volumetric Work, lb_f/s	η	Efficiency
p_{jet}	Static nozzle pressure	Λ	Taper ratio
p_0	Total pressure, *psi*	ρ	Density, lb/ft^3
$p_{0,\infty}$	Free-stream stagnation pressure, *psi*	Ω	Angular velocity, $°/s$

Acronyms

AAVP	Advanced Air Vehicles Program	CRM	Common Research Model
BL	Boundary Layer	DLR	German Aerospace Center
BLI	Boundary-Layer Ingestion	DPW	Drag Prediction Workshop
BWB	Blended Wing Body	JAXA	Japan Aerospace Exploration Agency
CAD	Computer Aided Design	NPSS	Numerical Propulsion System Simulation
CDISC	Constrained Direct Iterative Surface Curvature	TetrUSS	Tetrahedral Unstructured Software System
CFD	Computational Fluid Dynamics	USM3D	Euler and Navier-Stokes flow solver

I. Introduction and Background

ONE of the goals of the NASA Advanced Air Transport Technology Project as part of the Advanced Air Vehicles Program is to investigate technologies that may be able to improve flight performance for next-generation aircraft. Boundary-Layer Ingestion (BLI) is one such technology that has gained traction in recent years and is the focus of this paper. The concept of BLI is not new, with the first works published in the mid 1940s. In one of these early studies, Smith and Roberts [1] examined an aircraft that used suction slots located along the wing and fuselage to ingest the boundary layer in order to prevent or delay turbulent transition. In his study, Smith compared three engine configurations for the aircraft: a turbojet engine with boundary-layer suction, a turbojet, and a turboprop engine. Smith and Robert's tests showed that the engine, which included BLI, had a reduced fuel consumption of almost 33 percent, as well as an increased C_L and L/D compared to the turbojet without boundary-layer ingestion for the same aircraft.

In the 1970s, Douglass [2] conducted a study of aircraft with and without BLI. Although Douglas made some assumptions about the compressibility of the flow, inlet losses, and the conditions at which flow entered the engine, he was able to show that the BLI resulted in a reduction of the kinetic energy of the wake and the jet, resulting in a propulsive efficiency improvement of 16 percent over the noningesting aircraft.

In the 1980s, Goldschmied [3] designed a small integrated, self-propelled wind-tunnel model using a concept referred to as the Goldschmied propulsor. This propulsor included a slot around the aft portion of the fuselage to allow for boundary-layer ingestion. Wind-tunnel testing was conducted with this model, both in an unpowered and in a boundary-layer ingesting configuration. Using the data collected from the wind tunnel, Goldschmied was able to show that ingesting the boundary layer allowed for a propulsion power reduction of 50 percent over the unpowered configuration; however, a recent attempt to reproduce these wind tunnel test results for propulsion power reduction at the California Polytechnic State University wind tunnel using a Goldschmied propulsor proved unsuccessful [4].

More recent studies have combined BLI technology with blended wing body (BWB) geometry configurations in order to reduce specific fuel consumption for the aircraft [5-7]. These studies all show a reduction in the mechanical power required by the propulsor as compared to a typical podded nacelle configuration.

A recent experimental investigation conducted by Sabo and Drela into the merits of BLI using an electric ducted fan propulsor mounted behind an NACA 0040 body of revolution showed a power savings benefit of 25 percent over the baseline, non-BLI case [8].

There have also been several studies focused on assessing and reducing flow distortions at the fan inlet face, which could affect engine efficiency and therefore, overall performance of a BLI system [6,9,10]. However, the present study focuses on quantifying the aerodynamic benefit of BLI for the Common Research Model (CRM) geometry rather than BLI effects on engine performance. The main objective of this paper is to computationally verify if there is any benefit in terms of reduced propulsive power requirements and drag reduction to be gained from implementing BLI on a conventional commercial aircraft geometry, as well as to quantify and make a first-round attempt to improve on any such benefit. The principle success criteria for this work are to determine whether such a system might yield a net aerodynamic or propulsive benefit and whether this topic warrants additional study.

II. Boundary-Layer Ingestion Theory (Quasi One-Dimensional)

The main principle of this BLI concept for the purpose of this study is to reduce the overall propulsive power required by the aircraft by integrating an additional propulsor in the aft section of the fuselage where the low-velocity boundary layer can be ingested by the engine intake.

The BLI concept is derived from the more general concept of wake ingestion, which has been in use in marine propulsion for a number of years [11]. By re-energizing the wake produced by the airframe through the use of boundary-layer ingestion, overall energy losses can be decreased, thus allowing the aircraft to move through the air with less propulsive power than would be required with current podded nacelle configurations. The potential benefit of BLI can be explained by considering three configurations (as shown in Fig. 1). Fig. 1(a) shows shows a typical, underwing podded nacelle geometry with no boundary-layer ingestion (Baseline Configuration). Fig. 1(c) shows an ideal BLI configuration with only a BLI propulsor near the aft end of the aircraft. Fig. 1(b) shows a more realistic configuration with both underwing and BLI propulsors (Actual BLI Configuration). While none of these idealizations consider the interaction of BLI with the induced-drag span loading required for overall minimum drag, which of course must be done for any real applications, in this study the propulsor effects are isolated for the purpose of gaining a better understanding of BLI and its potential benefits.

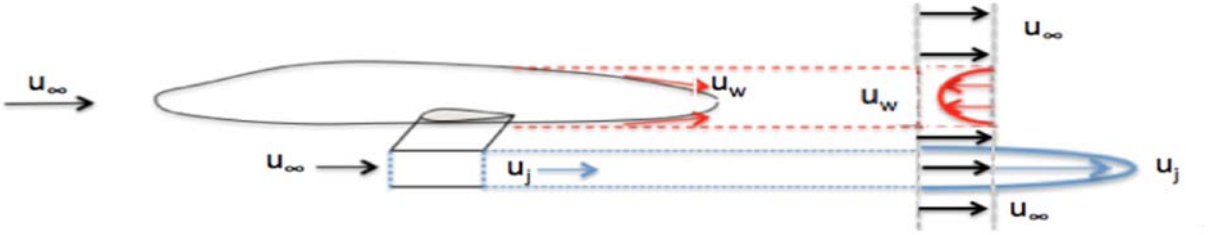

(a) Baseline configuration

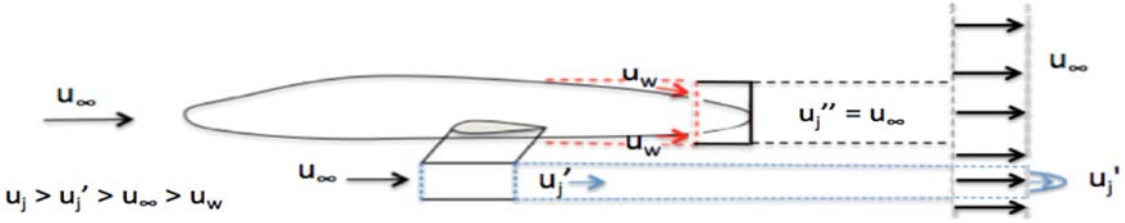

(b) Actual BLI configuration

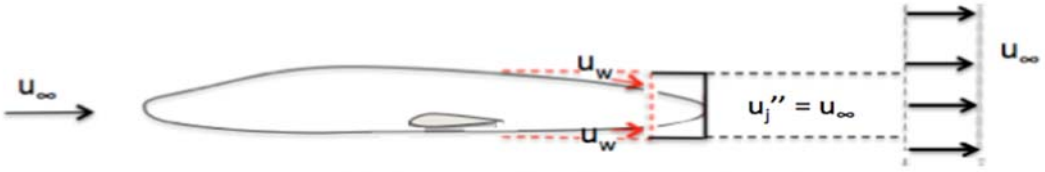

(c) Idealized BLI configuration

Figure 1: Simplified conceptual BLI benefit.

Derivation of non-BLI Power Requirements

In the Ideal BLI configuration, it is assumed that one hundred percent of the wake is ingested by the propulsor and that the wake is perfectly filled. However, as it would likely not be possible, nor beneficial to ingest one hundred percent of the developing boundary layer/wake, the actual BLI configuration would require supplemental propulsion from an underwing nacelle, as shown in the Actual BLI Configuration (Fig. 1(b)). In addition, there would likely be a variety of safety issues that would arise from a configuration with just a single BLI propulsor. Although the focus of this work is on an 'Actual' BLI configuration with both BLI and underwing propulsors, for simplicity, the following derivation will compare the Baseline Configuration (Fig. 1(a)) to an Ideal BLI Configuration (Fig 1(c)). The drag from the wing was ignored in all cases, as the focus of this work is fuselage boundary layer ingestion.

For the typical podded nacelle geometry, the airflow enters the engine at free-stream velocity, u_∞. The engine then accelerates the flow to a velocity u_j, which is higher than free-stream velocity in order to balance out the momentum deficit created by the airframe drag. For the BLI geometry, instead of ingesting the free-stream flow, the engine ingests the slower moving boundary-layer flow, u_w, and accelerates the flow up to free-stream velocity, u_∞. The potential benefit of a BLI system is derived from the difference in required energy input between BLI and non-BLI geometries

by the aircraft engines to achieve the same net axial force [12,13]. This benefit can be assessed starting with the general thrust equation

$$Thrust,\ T = (\dot{m} * u)_j - (\dot{m} * u)_\infty + (p_j - p_\infty) * A_j \tag{1}$$

where p_j and p_∞ are defined as the exit and free-stream pressures, respectively. The area A_j is defined as the jet exit area and u_j and u_∞ are the jet exit velocity and free-stream velocity, respectively. For a gas turbine engine, the nozzle of the turbine is usually designed in such a way as to make the exit pressure equal to free-stream pressure. In this case, the pressure-area term of the general thrust equation equals zero and can be dropped. The thrust equation can then be written as

$$T = (\dot{m} * u)_j - (\dot{m} * u)_\infty \tag{2}$$

To simplify, the added fuel used for combustion and the bleed air is neglected. Thus, the exit mass flow rate is assumed to be equal to the free-stream mass flow rate. For cruise, the total thrust is equal to the drag force, D_A, on the aircraft. From this, Eq. (2) can be rewritten as

$$T = \dot{m} * (u_j - u_\infty) = D_A \tag{3}$$

Since there is no change in potential energy of the system, the total mechanical energy added to the system is equal to the kinetic energy, added to the system by the engine, which can then be written as

$$E_{Mechanical,added} = \frac{1}{2} * m * {u_j}^2 - \frac{1}{2} * m * {u_\infty}^2 = \frac{1}{2} * m * ({u_j}^2 - {u_\infty}^2) \tag{4}$$

The rate at which this mechanical energy is added to the flow, power (*P),* can be obtained by substituting in the mass flow rate, $\dot{m}$.

$$P_{added,non-BLI} = \frac{1}{2} * \dot{m} * (u_j^2 - u_\infty^2) \tag{5}$$

Substituting Eq. (3) in the above yields

$$P_{added,non-BLI} = T * \frac{u_\infty + u_j}{2} \tag{6}$$

which is the power added to the flow to achieve cruise in the non-BLI case.

Derivation of BLI Power Requirements

For the BLI concept, the assumption is made that one hundred percent of the boundary layer is ingested by the engine and accelerated back up to free-stream velocity. In addition, it is assumed that the non-BLI and BLI cases will have equivalent mass flow rate. This assumption will be discussed in further detail in subsequent sections. Starting with Equation (3), but substituting in for the BLI case gives

$$T = \dot{m} * (u_\infty - u_w) = D_A \tag{7}$$

where u_w is the velocity of the ingested wake and u_∞ is equal to the BLI exit velocity, u_j'', as shown in Fig 1(c). Following the same substitutions, the total mechanical energy added to the system for the BLI case is

$$E_{Mechanical,added} = \frac{1}{2} * m * {u_\infty}^2 - \frac{1}{2} * m * {u_w}^2 = \frac{1}{2} * m * ({u_\infty}^2 - {u_w}^2) \tag{8}$$

By replacing m with $\dot{m}$ and substituting Eq. (7) into Eq. (8), the power added to the system can then be defined as

$$P_{added,BLI} = \frac{1}{2} * \dot{m} * (u_\infty^2 - u_w^2) = \frac{T}{2} * (u_w + u_\infty) \tag{9}$$

Simplifying

$$P_{added,BLI} = T * \frac{u_w + u_\infty}{2} \tag{10}$$

Since $u_w \leq u_j$, a comparison of Eqs. (6) and (10) shows that

$$P_{required,BLI} < P_{required,non-BLI} \tag{11}$$

From this, assuming the same mass-flow rate, $\dot{m}$ for the Ideal boundary-layer ingestion configuration as the conventional configuration, it is evident that less propulsive power is required by the Ideal boundary-layer ingestion configuration than for the conventional underwing configuration to maintain the same axial force.

The difference in energy input between the BLI and non-BLI scenario arises due to the fact that the flow entering the engine is at a lower velocity. Since less power is required for the BLI configuration, then substituting Eqs. (6) and (10) into Eq. (11), we get

$$T_{BLI} * \frac{(u_w + u_\infty)}{2} < T_{non-BLI} * \frac{(u_\infty + u_j)}{2} \tag{12}$$

or

$$T_{BLI} < T_{non-BLI} * \frac{(u_\infty + u_j)}{(u_w + u_\infty)} \tag{13}$$

The assumption of equal mass-flow rates for the BLI and non-BLI cases does not hold when trying to directly compare a BLI propulsor to a propulsor in free-stream flow. The boundary-layer flow will have a lower mass-flow rate by virtue of its velocity being lower than that of the free-stream flow. The assumption of equal mass-flow rates is instead based on the notion that the BLI propulsor will only be able to ingest a certain percentage of mass flow compared to the free-stream propulsor. This percentage of the free-stream mass-flow rate is assumed to be the point of comparison for the equal mass-flow rate assumption in the equations above. For example, if it is assumed that a free-stream propulsor has a mass flow rate of 20 kg/s but a BLI propulsor can ingest only 5 kg/s, then the 5 kg/s is assumed to be the point of comparison for equal mass-flow rates, $\dot{m}$, in the equations above.

It is important to note, the analysis above does not take into account various losses that would be expected due to the nonuniform velocity distribution of the boundary layer, various engine efficiencies (fan, compressors, etc.), increases in wetted area due to implementation of a BLI system [16] and interaction of the BLI system with the induced-drag span loading. More details on the quasi-1D and 2D analyses can be found in Refs. [14] -[17].

III. Baseline Geometry and Engine Model Generation – Underwing

The baseline geometry used for the purposes of this study is the Common Research Model (CRM) [18]. The Common Research Model was developed by a consortium of both public and private sector groups including, but not limited to, Boeing, Cessna, JAXA (Japan Aerospace Exploration Agency) and DLR (German Aerospace Center), in conjunction with NASA in order to help develop computational fluid dynamics (CFD) applications and validate their results.

The Common Research Model geometry itself is representative of a typical transonic transport aircraft designed for a Mach number of M=0.85 with a nominal lift coefficient of C_L=0.50, a Reynolds number of Re_c=40 million (based on a reference chord, C_{ref} = 275.80 inches), and an aspect ratio of AR=9.0. The geometry and data, including all wind-tunnel tests and CFD results, associated with the Common Research Model (CRM) are all open-source and available to the public [18]. Table 1 presents a list of basic reference quantities for the CRM.

Table 1: Reference quantities for CRM geometry.

S_{ref}	594,720.0 in^2
Trap-Wing Area	576,000.0 in^2
C_{ref}	275.80 in
Span	2313.50 in
X_{ref}	1325.90 in
Y_{ref}	468.75 in
Z_{ref}	177.95 in
Λ	0.275
AR	9

The most recent baseline CRM geometry consists of a tube-like body, wing, nacelle, pylon, and horizontal tail. However, there are various configurations of the CRM geometry available that do not include some of these features [19].

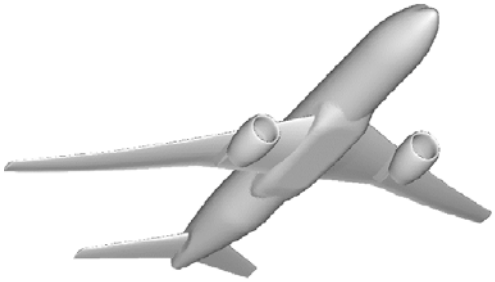

Figure 2: Full Common Research Model geometry.

For the purposes of this study, a semispan geometry, based on Fig. 2, consisting of the aircraft fuselage, wing, underwing nacelle, and horizontal tail is used. A semispan model is used in order to save computational resources. The boundary-layer ingesting system will be placed downstream of the horizontal tail. At this time, the underwing nacelle on the CRM is flow-through only and does not have any internal engine geometry.

In order to determine the existence of and quantify any potential benefit that might arise through the use of BLI, it is necessary to develop a working engine model for the underwing engine. The USM3D flow solver, which will be discussed in subsequent sections, allows for the modeling of jet engines through the use of inflow, core outflow, and fan bypass outflow boundary conditions defined on the solid model geometry prior to grid generation. As the CRM model currently uses flow-through nacelles and does not have any engine geometry, a model based on publically available engine geometry for the GE90-115B, the PAX300 will be added to the CRM underwing nacelle [20].

The internal engine geometry consists of an inlet hub, inflow plane (green), core exit (red), bypass fan exit (yellow) and plug sections as shown in Fig. 3.

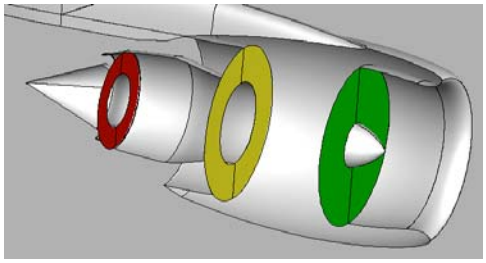

Figure 3: Internal view of underwing nacelle geometry and boundary condition planes. (red: core exit; yellow: bypass fan exit; green: inflow plane)

It is not necessary or practical to model the various compressors, ducts, and other components of the engine in USM3D, as this is done in the Numerical Propulsion System Simulation (NPSS). Engine conditions are specified by the user and applied to the core exit and bypass fan exit faces of the engine [21].

The inflow engine parameters are determined automatically within USM3D through a mass-flux balance method, with the fan and jet flows determined by adjusting the average back pressure across the inlet face. Using an averaged back pressure, the mass flux is balanced and distortion on the plane is maintained. The outflow conditions for the

engine are determined through nondimensional user-prescribed inputs for the static nozzle pressure. These six variables, three for each exit section, are calculated using the NPSS model and input into USM3D.

The PAX300 NPSS engine model, developed at NASA Glenn and used previously to model a GE90-115B similar engine [22] is used to generate the above USM3D inputs. The amount of thrust that the engine model produces is throttled in order to attain cruise conditions and provide a point of comparison between the BLI and non-BLI systems. Figure 4 shows a schematic of the engine geometry.

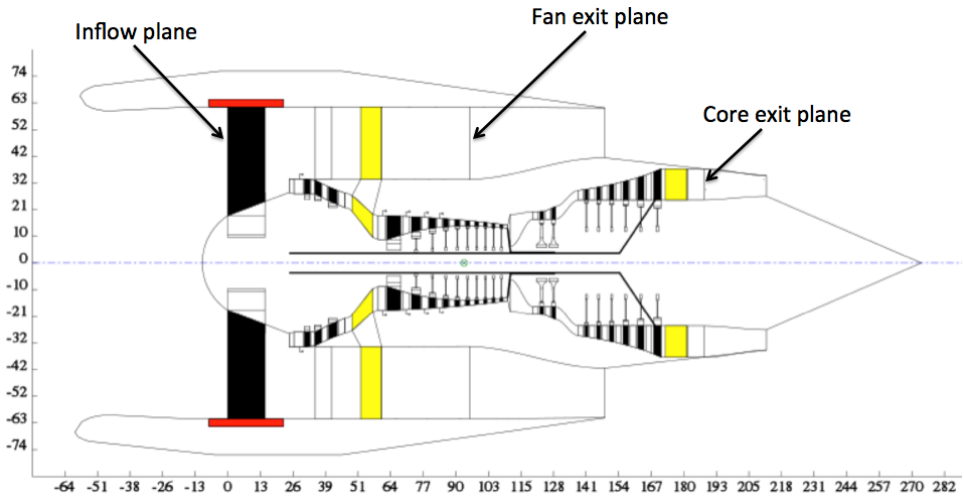

Figure 4: Geometry of NPSS model (inches).

Fig. 5 shows the semispan CRM with added internal engine geometry, which serves as the baseline geometry for this study. An open actuator disc, which will be discussed further in the following sections, is used to model the BLI system.

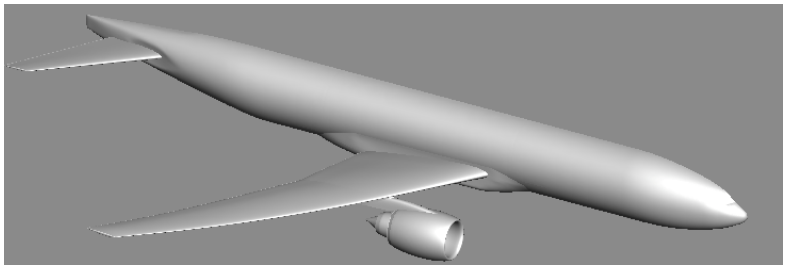
Figure 5: Baseline geometry – the Common Research Model with internal engine geometry.

IV. Assessing the BLI Benefit

To assess the potential benefit of BLI, the baseline geometry with underwing engines, shown in Fig. 5, is compared to the integrated BLI geometry, shown in Fig. 6. Computations are performed for both the baseline and BLI geometries and compared to determine the potential BLI benefit. This benefit will be assessed via the power balance method outlined by Drela [23].

Fig. 6 also illustrates how the BLI system interacts with the induced drag and wake generated from the wing and horizontal tail. The wake layer and wingtip vorticies generated by the wing is shown in solid red arrows, while the wake and horizontal downwash generated by the horizontal tail is shown using dotted red arrows. Note that the wakes from the underwing engines are not shown, as they are assumed to be far enough away to not interfere with the BLI system or the ingested wake coming off the aircraft fuselage. The velocity distributions for slices outboard of the wing and directly behind the BLI system are shown in blue. As the BLI system is located near the tail of the aircraft, only the flow coming directly off the horizontal tail and fuselage will be affected, leaving much of the induced drag and wake generated further outboard of the wing unaffected. As can be seen in Fig. 6, the wake region downstream of the BLI system is reduced compared to the wake region further outboard on the wing. For the non-BLI case, there will be no wake filling behind the fuselage and the velocity distribution behind the fuselage will be much closer to that of the

mid-span velocity distribtuon shown. The viscous wake region downstream of the wing causes a decrease in velocity, denoted as u_{wake} compared to free stream velocity, u_∞. The velocity distribution for the region directly downstream of the BLI system shows that the velocity deficit that would normally be present, denoted as $u_{\text{filled wake}}$ can be reduced or eliminated.

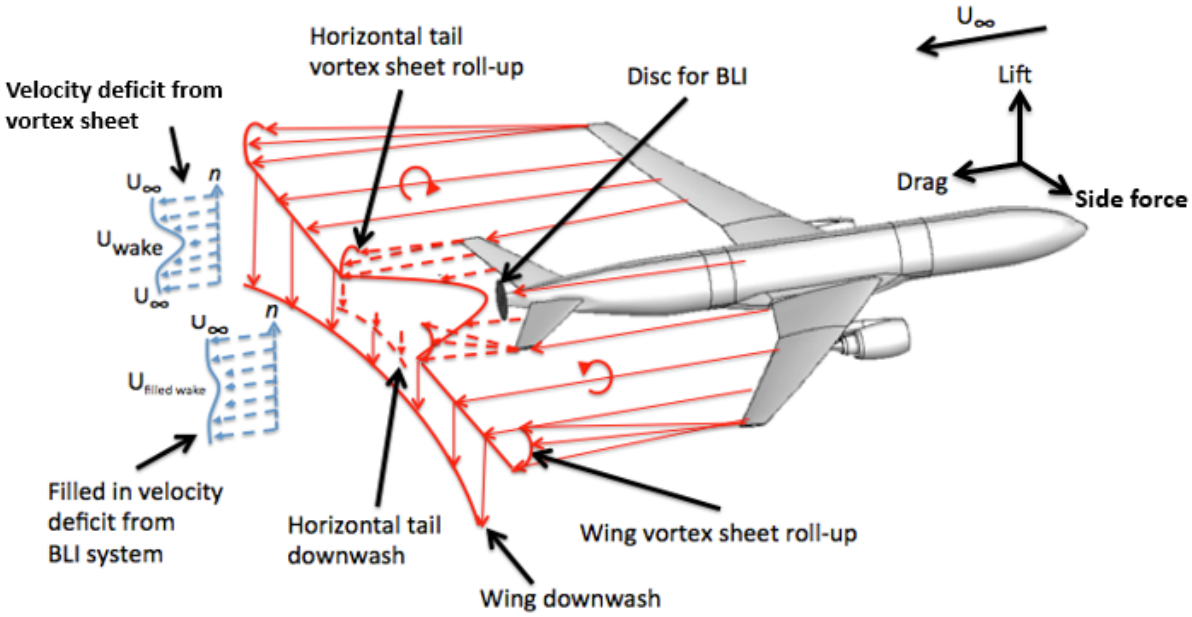

Figure 6: Schematic of the Common Research Model with BLI disc.

For this method, the benefit of BLI will be derived from reducing the power dissipation in the overall flow field by reducing streamwise velocities and kinetic energy losses due to the boundary layer on the fuselage producing a low momentum wake behind the vehicle. This is accomplished by filling in the wake generated by the airframe with the BLI propulsor, as shown simplified in Fig. 1(b) and Fig. 6. This power balance method allows for the complete quantification of boundary-layer losses and propulsor losses of the aircraft, rather than separating out the thrust and drag forces on the aircraft. The potential benefit of a BLI system is likely to be affected by the fan performance of the engine due to distorted flow at the inlet of the propulsor. Drela's power balance method allows for the separation of the fan efficiency from the propulsive efficiency of the aircraft, thus allowing for direct assessment of potential benefit. Since this is a CFD study, we will also be able to pull out the thrust and drag components and compare to the power balance method results.

There are three sources of mechanical power within a flow field as outlined by Drela: P_k, which is the net mechanical power across the propulsor inflow and outflow faces, P_s, which is shaft power from moving surfaces, and P_v, which is the power due to the volumetric work within a flow field. For a control volume encompassing the propulsor and in the low-speed case, the only flow-field power source left is P_k, which can be defined as the volume flux of total pressure across the inflow and outflow faces of the engine

$$P_k = \oiint \left(p_{0_\infty} - p_0\right) V \cdot \hat{n}\, dS \tag{14}$$

where p_0 is the total pressure at the engine face, p_{0_∞} is the free-stream total pressure, V is the inlet velocity at the propulsor face, and $\hat{n}$ is the vector normal to the fan face. The area integral is taken over both inflow and outflow propulsor planes, so P_k is a measure of net engine flow power while internal propulsor losses are irrelevant, allowing the engine fan efficiency to be separated from the aerodynamics of the BLI geometry [23].

For this study, we define the drag coefficient, C_D, as the summation of all the force components in the streamwise direction on all solid surfaces of the vehicle. We define the thrust coefficient, C_T, as the summation of the forces on the inlet and exit planes of the propulsors, also in the streamwise direction (this assumes that the engine is aligned with the flow at the cruise condition). The coefficients C_D and C_T are defined as follows

$$C_D = \frac{F_{x,Solid}}{q_\infty S_{ref}}, \quad C_T = \frac{F_{x,inlet\&exit\ planes}}{q_\infty S_{ref}} \tag{15}$$

where q_∞ is the free-stream dynamic pressure and S_{ref} is the reference area of the geometry (typically, the wing planform area).

The net force coefficient in the streamwise direction, C_X, is then defined as the thrust coefficient, C_T, minus the drag (force) coefficient, C_D.

$$C_X = C_T - C_D \tag{16}$$

With the net propulsor power coefficient defined as follows

$$C_{P_k} = \frac{P_K}{q_\infty V_\infty S_{ref}} \tag{17}$$

and as S_{ref} may change between geometry iterations, this allows for an effective comparison between non-BLI and BLI geometries using the net mechanical power, P_k defined previously by Eq. (14).

The aerodynamic benefit of the BLI system can be expressed as follows

$$BLI\ benefit = \frac{(C_{p_k})_{non-BLI} - (C_{p_k})_{BLI}}{(C_{p_k})_{non-BLI}} \tag{18}$$

V. Computational Tools

Several different computational tools, outlined below, were used for this study.

Grid Generation

The surface triangulations along with the field tetrahedral volume grids were generated using the GridTool and VGRID software developed at Langley Research Center [24]. GridTool serves as a connection between Computer Aided Design (CAD) software and grid generation software such as VGRID. In GridTool, surface patches are defined along the configuration by the user, source terms are places throughout the domain for grid generation, and domain boundaries for the model are defined. A rectangular box that encompasses the geometry is used to define the computational domain and far-field boundaries. Each face of this rectangular box is located ten body lengths away from the configuration in the upstream, radial, and downstream directions. The output from GridTool is used to automatically generate the computational domain using VGRID. VGRID uses an advancing front method for generating Euler tetrahedral grids and an advancing layers method for thin-layer viscous grid generation for Navier-Stokes analysis. As a general practice, each final converged solution is analyzed to ensure that the viscous sublayer, has been grid resolved and that the average y^+ is less than 1.

Numerical Propulsion System Simulation

NPSS is a component-based, object-oriented, engine cycle simulator capable of simulating the aerothermodynamic cycle for gas turbine engines and other complex systems. The system uses a linked building block approach to define system configuration that allows for single and multipoint design, as well as steady-state and transient analyses. NPSS focuses on the integration of aerodynamics, structures, and heat transfer along with the concept of numerical zooming between zero-dimensional, one, two, and three-dimensional engine codes [25,26]. An engine model similar to the GE90-115B, the PAX30021, [22,27] will be used in this work to generate engine conditions for the underwing engine for use in CFD analysis.

USM3D Flow Solver

USM3D is a tetrahedral cell-centered, finite-volume, Euler and Navier-Stokes flow solver. Time integration follows the implicit point Gauss-Seidel algorithm, explicit Runge-Kutta approach, and local time stepping for convergence acceleration [21]. For this study, Roe's flux-difference splitting (FDS) method along with the Spalart-Allmaras turbulence model with no flux limiter is used. Separate core, bypass, and inflow boundary conditions are used to model the underwing engine. Inflow engine parameters are determined automatically within USM3D through a mass-flux balance method with the fan and jet flows by adjusting the average back pressure across the inlet face.

Using an averaged back pressure, the mass flux is balanced, and distortion on the plane is maintained. The outflow conditions for the engine are determined through nondimensional user-prescribed inputs for static nozzle pressure, p_{jet}, stagnation pressure of the jet, p_{0jet}, and stagnation temperature of the jet, T_{0jet}, for both the core and bypass fan flows. These user-prescribed inputs are calculated from NPSS model output.

Constrained Direct Iterative Surface Curvature

CDISC is a knowledge-based inverse design approach. An overview of the CDISC design process is presented in Fig. 7. Geometry and flow information from a preliminary analysis are passed from the flow solver to the CDISC module. Surface coordinates and pressure coefficients are extracted from the analysis, and an initial set of target pressures are generated using the current analysis pressures. These target pressures are automatically adjusted to meet the input flow constraints, and a new surface geometry is obtained. The volume grid is then modified based on surface geometry changes and input back into the flow solver for further analysis. This iterative process repeats until the extracted surface pressures match input target pressures [28].

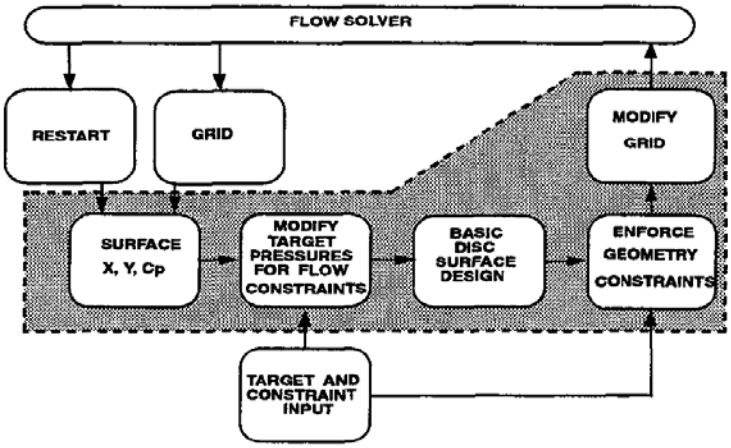

Figure 7: CDISC system flow chart [28].

VI. Methodology Overview

Before the simulations relating to BLI were carried out, a verification study of the computational model was completed and compared to previously obtained numerical and experimental data in order to ensure that the results obtained relating to BLI could be considered accurate. The full results of the verification study can be found in the Refs [17, 29-32].

In order to determine the aerodynamic effects and potential benefits of a BLI system on the Common Research Model (CRM), several different iterations of the CRM geometry were used. The baseline geometry consisted of an unaltered semispan CRM geometry incorporating an underwing nacelle with added internal engine geometry, as shown in Fig. 5. Unstructured viscous grids were generated using NASA Langley's GridTool and VGRID grid generation packages. The Numerical Propulsion System Simulation (NPSS) software was used to simulate an engine cycle similar to that of the GE90-115B gas turbine engine at cruise conditions using publicly available data. This engine simulation was used to determine the engine inlet and exit boundary conditions for the underwing nacelle. USM3D was used as the flow solver. Each geometry was run for a total of 25,000 iterations on the NASA Pleiades supercomputer in order to ensure solution convergence. The model was run at cruise conditions of Mach 0.85 at an altitude of 38,500 feet, a Reynolds number of 40 million based on mean aerodynamic chord with 2° angle of attack and no sideslip condition. As outlined previously, net propulsor power and net horizontal force coefficients were calculated.

After the baseline calculations were completed, the CRM geometry was altered to incorporate the BLI system. For this, an actuator disc was placed at the approximate fan location slightly downstream of the empennage to represent the BLI system, as shown in Fig. 6. The rest of the geometry, including underwing nacelle, remained unchanged. The same cruise conditions outlined above were used and once again, the net propulsor power, net horizontal force, and drag coefficients were calculated.

Once the first BLI run was completed, the aft portion of the fuselage of the BLI-integrated geometry was modified in an attempt to optimize the flow and potential benefits of the system. The exact changes to the geometry are discussed in detail in later sections. These changes to the BLI geometric design were made using CDISC [28].

Once all of the simulations were completed, any aerodynamic or propulsive power savings benefit from the BLI system as compared to the non-BLI configuration were determined. An assessment of the BLI concept for this application was made and future work recommended.

VII. Methodology for Comparison of Baseline (Non-BLI) and BLI Geometries

For an equivalent mass-flow rate, it was shown in Section II that a BLI system requires less propulsive power than a conventional non-BLI system. However, since the BLI system by definition ingests the slower-moving boundary-layer air, it is difficult and impractical to actually design the BLI system in such a way as to have the same mass-flow rate as that of an underwing engine. Instead, as a way to supplement thrust generated by the underwing engines instead of attempting to replace them, the BLI system is constrained to ingest only the mass flow present in the developing boundary layer and accelerate it up to free-stream velocity This has several implications: 1) a portion of the overall required thrust for cruise will now be produced more efficiently by the BLI system compared to the underwing engine, 2) the underwing engine now needs to produce less thrust overall since the BLI system is contributing a portion of the total thrust required, which should reduce the amount of propulsive power required by the underwing engine, and 3) since the BLI system is ingesting and accelerating the boundary-layer air, there should be some benefit in terms of reduced drag on the fuselage that would not be present in a conventional propulsive system, although this will likely be dependent on the actual geometry alterations made to incorporate the BLI system. In this case, the underwing engine could possibly be made smaller, thus further reducing aircraft weight and drag and increasing the overall benefit of the BLI system.

In order to fairly compare the required propulsive power for the BLI and non-BLI systems in cruise, the net streamwise force coefficient, C_X, is constrained to be zero for all configurations. C_X is computed by summing the streamwise component of the integrated pressure and viscous forces on all airframe surfaces. The BLI engine is modeled to ingest the developing boundary layer and accelerate it up to free-stream velocity, while the underwing engine is modeled using the parameters derived from the NPSS model and adjusted to achieve a zero net streamwise force for the aircraft. It should be noted that this is a simplification. In reality, the image in Fig. 1(b) will occur. Hence, a BLI system would accelerate the flow leaving the fuselage up to or exceeding freestream velocity, but a conventional underwing (non-BLI) engine would still be required to maintain flight (albeit at a reduced power setting).

VIII. Underwing Engine Model CFD Results

The semispan CRM geometry with underwing nacelle and internal engine geometry, discussed previously in Section III, was used as the baseline geometry for this study. Cruise conditions as outlined in Section VI were used for the simulation. All simulations were conducted at a Reynolds number of 40 million based on mean aerodynamic chord.

While the main focus of this work is not to redesign or optimize the underwing engine, the ability to couple the NPSS raw output with the USM3D flow solver to produce a realistic representation of a high bypass turbofan engine is a key part of determining proof-of-concept for BLI in this application.

Fig. 8(a) shows a two-dimensional, centerline cut through the underwing engine. From this, it can be seen that the flow-through engine inlet is subsonic with no shocks apparent. Fig. 8(b) shows a Mach contour at the engine inlet face with a maximum Mach number of less than 0.6, indicating a good inlet design. The exit flow is close to Mach 1, which is desirable for high bypass turbofan engines. In addition, there does appear to be a small low-speed zone near the engine plug, which could be reduced by making the plug larger. However, as this zone is relatively small and the intent is to investigate BLI and not optimize the underwing engine, the plug dimensions will remain unchanged. Overall, the NPSS model yielded good results and allows for a reasonable assessment of BLI in this application.

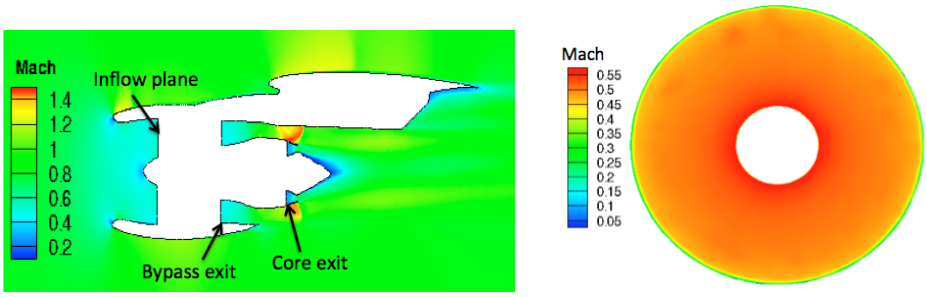

(a) Side-view (b) Inlet face

Figure 8: Underwing engine, Mach number contour plot, (Re_c=40 million, M=0.85, $\alpha = 2°$).

IX. Baseline Geometry CRM and Underwing Engine Model CFD Results – Power and Thrust

As defined in Section IV, drag, thrust, and net propulsor power coefficients were calculated for the baseline geometry and are presented in Table 2. The net streamwise force coefficient, C_X, was computed over all surfaces (solid, as well as the propulsor inlet and exit planes). The drag coefficient, C_D, was computed over only the solid surfaces, and the engine power coefficient, C_{Pk}, and thrust coefficient, C_T, were computed over the engine inlet, bypass exit, and core exit faces. The amount of thrust that the engine model produces was throttled in order to gather the necessary data.

Table 2: Computed net streamwise force, drag, thrust, and engine power coefficients for the baseline (i.e. non-BLI) configuration (Re_c=40 million, M=0.85, $\alpha = 2°$).

C_X	C_D	C_T	C_{Pk}
-0.00066	0.03217	0.03151	0.986
0.00034	0.03112	0.03146	0.832
0.00133	0.03007	0.03140	0.682

From Table 2, when C_X is negative, the vehicle has less thrust than is needed to compensate for the drag and thus, the vehicle will decelerate. When C_X is positive, the vehicle accelerates because the drag is less than the thrust. It is not possible to refine the engine conditions any further between these two points due to engine model fidelity, so an estimate of C_{Pk}, C_D, and C_T at the exact cruise point of $C_X = 0$ must be interpolated from available data. From the data, an engine power coefficient of $C_{Pk} = 0.878$, drag coefficient of $C_D = 0.03143$, and $C_T = 0.03143$ for the semispan baseline geometry at cruise conditions are computed. In addition, a nominal value of $C_L = 0.411$ was calculated across all engine conditions.

X. BLI Geometry – Boundary-Layer & Actuator Disk Implementation

In addition to the coefficients computed above, it is also necessary to investigate the developing boundary layer and wake produced by the aircraft in order to implement a BLI system. The boundary layer/wake thickness was approximated following the contour of the developing boundary layer along the fuselage and extending this contour into the wake region as shown by the black lines in Fig. 9.

As stated previously, for the purposes of this work, the slower-moving boundary-layer flow is ingested and accelerated to match the free-stream velocity. Since the exit velocity of the disc is specified to be free-stream velocity, there is no need to ingest free-stream air in this application. The radius of the disc can therefore be constrained so that it is not ingesting free-stream air, as areas of the disc in the free-stream would generate thrust by accelerating the flow to above free-stream velocity. Therefore, the radius of the disc is further confined to be the smallest distance from the center of the disc to the edge of the approximate boundary-layer edge location in any direction.

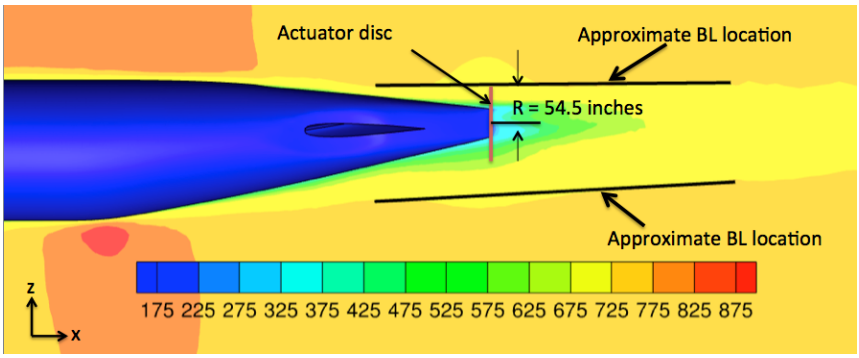

Figure 9: Velocity contour plot showing actuator disc constraint, x-z view, (Re_c=40 million, M=0.85, α=2°).

The constraining distance is calculated to be approximately 54.5 inches, which is the distance from the center of the disc to the upper edge of the approximated boundary layer in the z direction. For the full model, this gives the actuator disc an area of 64.8 ft^2, with the ingested boundary layer having a mass-weighted velocity of 648.8 ft/s and mass-flow rate of 26.9 slugs/s. For comparison, the same size actuator disc placed in the free-stream has a mass-flow rate of 33.4 slugs/s.

Since the maximum exit velocity of the BLI system is constrained to be equal to free-stream velocity, there is a diminishing return on how large the system is versus how much benefit can be derived from it. Using the modified general thrust equation from Eq. (2), it is certainly possible to take flow at 99% u_∞, and generate thrust by imparting a slight acceleration. However, far more thrust and therefore, net benefit can be generated by taking the slower moving flow found deeper in the boundary layer and accelerating that to match u_∞, since this would create a larger Δu. The 'sweet spot' for how much of the boundary layer to ingest is largely dependent on the type of propulsion system, how efficient the system is, and what velocity constraints, if any, are placed on the exit flow; however, this is not the focus of this study. In addition, the larger the BLI system is, the larger the potential weight and drag penalties of implementing the system will be, with the latter ones being ignored in the present study.

Using Eq. (2), the ingested boundary-layer mass-weighted velocity of 648.8 ft/s as the inlet velocity, the mass flow rate of 26.9 slugs/s and constraining the exit velocity to match free-stream velocity, or 822.8 ft/s, the actuator disc is expected to produce 1,058 lb_f of thrust, approximately 10% of the total thrust required for cruise.

XI. BLI Geometry Results – First Iteration

For the initial BLI system, an open, full actuator disc as discussed previously was implemented on the full span CRM directly downstream of the fuselage with no alterations to the fuselage itself. A uniform step pressure increase was imposed across the surface of the actuator disc. This pressure increase was calculated internally in USM3D using the thrust coefficient defined in Eq. (19), the free-stream Mach number, M_∞, and user input for advance ratio, J. An advance ratio of 0.7 was chosen based on the radius of the actuator disc in order to keep the 'tips' of the disc subsonic. The thrust coefficient C_T was chosen in an attempt to completely fill in the wake behind the fuselage of the aircraft, based on a required estimated thrust force as described earlier in Section X.

$$\Delta C_{p,disc} = \frac{C_T * M_\infty^2}{J^2} \tag{19}$$

Fig. 10 shows a velocity contour plot of the flow coming into the actuator disc. From the contour plot, it is evident that the actuator disc is entirely immersed in the boundary-layer/wake of the aircraft; however, the velocity profile is not uniform. The top portion of the actuator disc has the fastest moving flow, with a maximum velocity of 775.8 ft/s. Relative to the top portion of the actuator disc, the sides and bottom have slower-moving flow due to interference from the horizontal-tail wake and the taper from the bottom of the fuselage. The center of the actuator disc where the fuselage terminates has a minimum velocity of 104.48 ft/s, approximately 12.7% that of free-stream velocity.

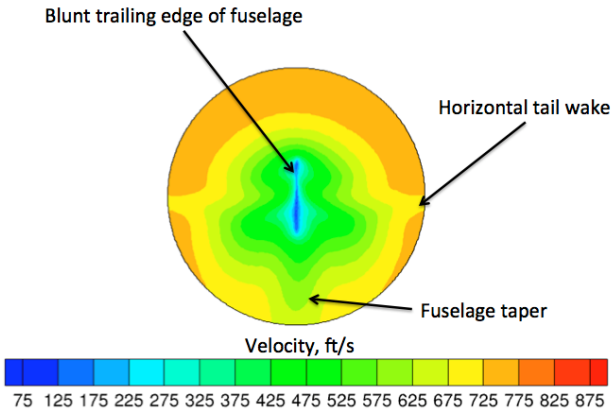

Figure 10: Velocity contour plot, BLI geometry actuator disc 'in' face, (Re_c=40 million, M=0.85, α=2°).

Fig. 11 shows a velocity contour plot of the wake regions for both the baseline and BLI geometries. The overall length of the wake region has been reduced, as well as the magnitude of the lower-velocity regions shown in green and yellow.

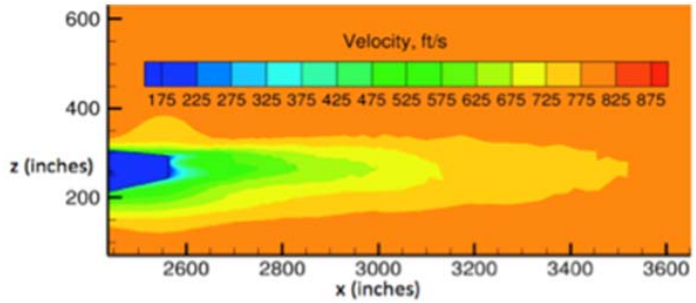

(a) Baseline geometry

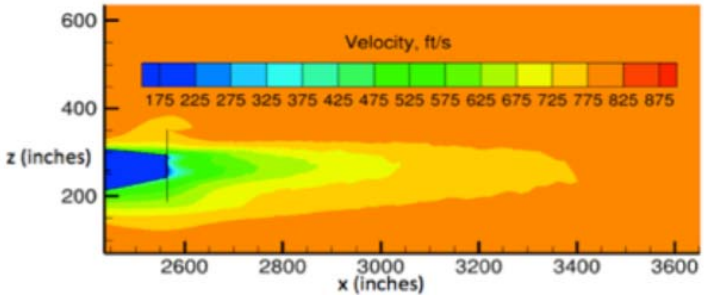

(b) BLI geometry

Figure 11: Velocity contour plot of wake regions, x-z view, (Re_c=40 million, M=0.85, α=2°).

It is evident that implementing the actuator disc does have a moderate effect on the aircraft wake, although it is not completely eliminated as intended. Fig. 12 shows an isometric view of the wake and actuator disc for the baseline and BLI geometries.

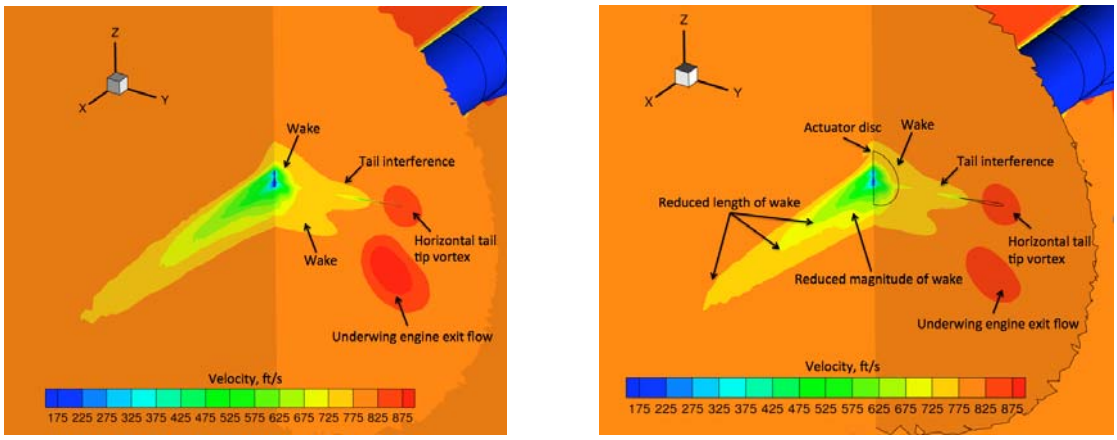

(a) Baseline geometry (b) BLI geometry

Figure 12: Velocity contour plot with slice at actuator disc location, BLI geometry, (Re_c=40 million, M=0.85, α=2°).

The actuator disc appears to be fully immersed in the wake/boundary-layer, although there is a large portion of the wake/boundary-layer flow that is not ingested by the actuator disc. Compared to the baseline geometry, the lower velocity regions, particularly the green and blue, which represent the lowest velocity areas, are all reduced in size and length. In addition, the overall length of the wake is reduced.

The engine power coefficient, C_{Pk}, and net streamwise force coefficient, C_X, were calculated for the BLI geometry and compared against previous results for the baseline geometry, shown in Table 3. Since it was not possible to refine the engine model any further between the data points, C_{Pk} at the exact cruise point of $C_X = 0$ was interpolated from available data.

The BLI configuration is shown to require approximately 8% less propulsive power relative to the baseline geometry. In addition, there is a reduction in the drag coefficient, C_D, of approximately eleven counts for the BLI geometry, likely due to the actuator disc accelerating the flow slightly as it nears the end of the fuselage, thus re-energizing the boundary layer and accelerating the wake flow back to freestream conditions. A nominal C_L value of 0.406 was calculated for the BLI geometry over all engine conditions, a reduction of 0.005 compared to the baseline geometry. The small change in C_L between the BLI and baseline geometries could likely be attributed to a slight acceleration and re-energizing of the boundary layer over the surface of the geometry upstream of the actuator disc.

Table 3: Computed engine power, drag, and lift coefficients for baseline and BLI geometries, (Re_c=40 million, M=0.85, α = 2°).

Geometry	C_{Pk}	Power Reduction	C_D	C_L
Baseline	0.878	-	0.03143	0.411
BLI	0.808	7.96%	0.03026	0.406

XII. BLI Geometry Results – Second Iteration

A preliminary attempt to improve the benefits of the actuator disc BLI system was made using the Constrained Direct Iterative Surface Curvature [28] (CDISC) design method by slightly altering the back portion of the fuselage near the actuator disc. CDISC works by extracting the surface coordinates and pressure coefficients from an initial analysis. Specific design target stations (e.g., a portion of the wing, an area of the fuselage), as well as target pressures, flow, and geometry constraints for these areas are designated by the user. CDISC then alters the geometry by stretching, shrinking, and moving the surface mesh cells in an attempt to match the desired target pressures along the designated design target stations. Once the surface geometry is altered, the volume grid is then modified based on the surface geometry changes and input back into the flow solver for further analysis. This iterative process is repeated until the extracted surface pressures match input target pressures [28]. For this design attempt, four target stations were used, located every 90 degrees circumferentially, starting from the top of the fuselage.

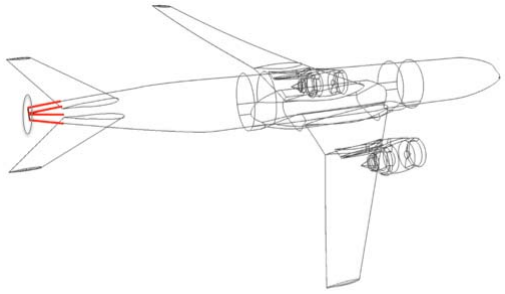

Figure 13: CDISC design stations (red).

Fig. 13 shows the design stations in red, beginning just downstream of the trailing edge of the horizontal tail and extended to the end of the fuselage. The final vertical thickness of the fuselage is held constant so that the geometry changes are not too drastic, as this is only a first-round design attempt.

The surface pressures for the original BLI geometry were extracted, and a constant C_p design constraint was imposed over the top and bottom of the fuselage to increase the average surface pressure of the design area. Because the empennage surface causes a boattail (or decreasing surface slope), an increase in pressure will cause a drag reduction or thrust component. Normally, this geometry change would be expected to decelerate the flow, increasing the boundary-layer and wake. However, as the BLI system is located close by, any decrease in velocity should actually be beneficial to the BLI system and contribute to the overall power reduction. No design constraints were imposed on the sides of the fuselage. However, as CDISC blends the geometry changes between the stations, the surface mesh was altered slightly at these locations. Fig. 14 shows the original surface mesh (blue) and redesigned CDISC mesh (red).

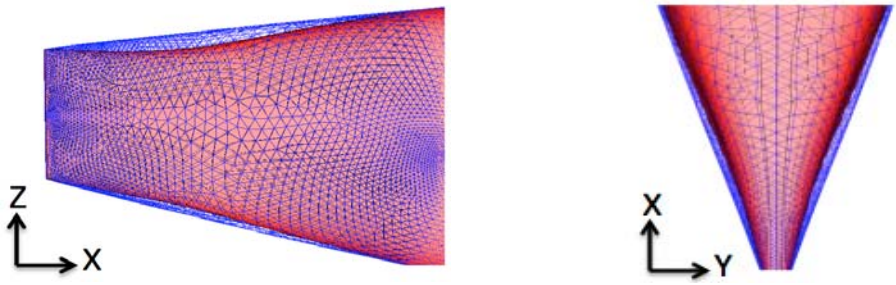

(a) Side view (b) Top view

Figure 14: Original mesh (blue) and CDISC mesh (red),

Again, the engine power coefficient, C_{Pk}, and net streamwise force coefficient, C_X, were calculated for the redesigned BLI geometry and compared to previous results for both the baseline and original BLI geometries, shown in Table 4. The redesigned BLI configuration is shown to require 8.7% less propulsive power relative to the baseline geometry, a 0.7% improvement over the original BLI geometry. There is a slight drag reduction of approximately twelve counts for the redesigned BLI geometry compared to the original BLI geometry. A nominal C_L value of 0.407 was calculated for the CDISC BLI geometry over all engine conditions, a reduction of 0.04 compared to the baseline geometry. This change in C_L is likely the result of a slight re-energizing of the upstream boundary layer flow caused by the actuator disc and changes made to the geometry using CDISC.

Table 4: Computed engine power, drag, and lift coefficients for baseline, BLI, BLI w/ CDISC and CDISC w/o BLI geometries, (Re_c=40 million, M=0.85, $\alpha = 2°$).

Geometry	C_{Pk}	Power Reduction	C_D	C_L
Baseline	0.878	-	0.03143	0.411
BLI	0.808	7.96%	0.03026	0.406
BLI w/ CDISC	0.802	8.7%	0.03022	0.407
CDISC w/o BLI	0.891	-1.4%	0.03169	0.411

Further alterations to the fuselage were not possible at this time due to a combination of geometric and grid constraints. CDISC works by stretching and shrinking cells on the surface mesh. This stretching and shrinking is then propagated out into the volume grid. However, since the actuator disc was located so close to the back end of the fuselage in this case, stretching and shrinking cells in this area resulted in negative volume cells and cells with crossed faces, which were not able to be removed. In order to correct this, it would be necessary to either regenerate the grids with a much finer mesh in the actuator disc area, which would allow surface mesh changes to propagate out into the volume grid without the creation of negative cells, or else the relocation of the actuator disc further away from the end of the fuselage.

As it is unclear at this point, whether the additional reduction in engine power requirements at cruise for the CDISC BLI geometry compared to the first iteration BLI configuration arises from improved performance of the fuselage itself, an increased benefit derived from the BLI system, or else a combination of both, an additional study was done to determine where this benefit comes from. To this end, the actuator disc representing the BLI system was removed from the CDISC geometry and the simulations rerun at the same cruise and engine conditions. The engine power coefficient, C_{Pk}, and net streamwise force coefficient, C_X, were calculated and compared to results obtained for all other geometries. The alterations made to the fuselage using CDISC without the BLI system resulted in an increase of the power required for cruise of 1.4% over the baseline, see Table 4. However, as stated previously, these same changes implemented in conjunction with the BLI system resulted in a power reduction of 0.7% between BLI geometries. In addition, there is an increase in the drag coefficient of approximately 2.6 counts between the non-BLI geometries. A nominal C_L of 0.411 was calculated, as well over all engine conditions.

Since the changes made to the geometry using CDISC resulted in a power reduction for the BLI geometry and an increase of power requirements for the CDISC altered, non-BLI geometry, it is safe to say that the increased reduction in power requirements for the CDISC BLI geometry is a result of increased BLI performance due to fuselage shaping.

A summary of results for engine power, C_{Pk} and drag coefficient, C_D, obtained in this study for all geometries are presented in Table 5 and in Fig. 15.

Results from this study indicate a propulsive power savings of 8.7% and a drag reduction of approximately twelve counts for the BLI geometry with CDISC compared to the baseline geometry.

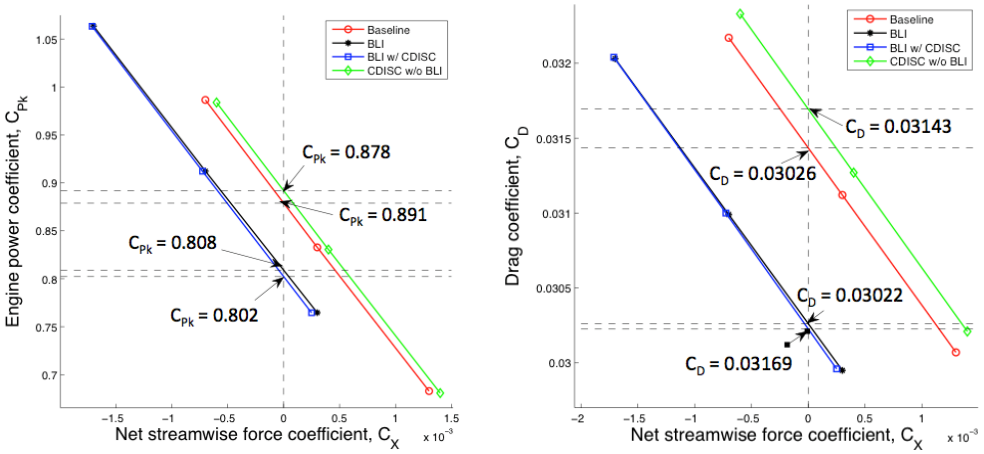

(a) Engine power coefficient (b) Drag coefficient

Figure 15: Net streamwise force coefficient versus: a) engine power coefficient, b) drag coefficient; for all geometries, (Re_c=40 million, M=0.85, α = 2°).

XIII. BLI Performance - Effect of Reynolds Scaling

An additional BLI study was conducted at a wind-tunnel scaled Reynolds number of 5 million using the same geometries and methodology, with more details documented in Ref [32]. Results from this study indicate a net cruise power reduction of 15.6% with a drag reduction of eighteen counts compared to the baseline geometry at the lower wind-tunnel Reynolds number. A summary of data for the lower wind-tunnel Reynolds number of the CRM experiment [18] from this study is presented in Table 5 below.

Table 5: Computed engine power, drag, and lift coefficients for all geometries, (Re_c=5 million, M=0.85, α = 2°).

Geometry	C_{Pk}	Power Reduction	C_D	C_L
Baseline	1.574	-	0.0389	0.378
BLI	1.348	14.4%	0.0372	0.374
BLI w/ CDISC	1.328	15.6%	0.0371	0.373
CDISC w/o BLI	1.545	1.8%	0.0386	0.377

From this, it becomes apparent that the Reynolds number scale and C_L variation for the same aircraft have a profound effect on the potential BLI benefits. It is reasonable to assume that the increase in BLI benefit is a result of both a benefit resulting from ingesting a thicker boundary layer and a higher baseline C_D, while operating at a lower C_L. It should be kept in mind that neither Re_c study summarized in Tables 4 and 5 has been optimized, yet the primary message being that the Reynolds scale is of upmost importance when evaluating potential BLI benefits.

XIV. Conclusions and Future Work

Unstructured grid-based computational solutions encompassing multiple geometries and several different computational tools have been demonstrated, along with a methodology for evaluating the benefit of boundary-layer ingestion for conventional aircraft. GridTool and VGRID advancing front grid generation software were used to generate unstructured tetrahedral grids for analysis.

The USM3D flow solver has been verified against both previous computational results and data gathered during earlier experiments using the Common Research Model geometry [17,29-31]. The NPSS software has been shown to provide useful inputs for CFD analysis, allowing for the realistic modeling of turbojet engines in this application. In addition, CDISC has been shown to be a useful tool for geometry modification and design.

From the analysis above, it is evident that the combination of BLI both with and without fuselage shaping provides a reduction in terms of propulsive power required for cruise. This benefit has been shown to be the result of a combination of wake filling and using the slower moving boundary-layer flow for propulsion instead of free-stream

air, as outlined in Section II. It is important to note that as the wake was only moderately reduced by the introduction of the BLI system, the majority of the benefit of BLI, in terms of cruise propulsive power reduction seems to stem from the reduction in velocity of the incoming flow into the propulsor.

The current BLI propulsor model imparts a uniform pressure jump across the actuator disc, which may not be entirely accurate when the fan encounters an inlet distortion. An actual fan would impart a smaller pressure rise to the portion of the flow with higher stagnation pressure and larger pressure rise to the portion of the fluid with lower stagnation pressure. These differences in pressure rise across the fluid could affect flow behavior upstream of the actuator disc, as well as the exhaust flow. The implementation of a more advanced actuator disc boundary condition with a radially varying pressure distribution is recommended to improve accuracy of results for BLI implementation.

As this study used a nondescript, open actuator disc propulsion system to model the BLI system, the implementation of a more real-world propulsion system would improve the trustworthiness of calculated potential benefits, as well as allow for evaluation of system-dependent losses. A trade study to determine a list of viable candidates (e.g., open propeller, ducted electric fan, small turbofan engine) using current technology, or the development of a specifically designed propulsion system and implementation of such a system, would yield more accurate results on the exact amount of power savings from the use of BLI as it is implemented here. The use of a full propulsion system model over the representative actuator disc would also allow for assessments of any weight penalties or reduction in benefits from flow distortion through the inlet, fan face, and/or nacelle depending on the chosen systems, as these are not modeled in this study.

In order to better understand the prospective power savings and how a BLI system might affect other subsystems and flight variables, additional computations should be conducted at alternate operating conditions and flight regimes.

Although the actuator disc boundary condition likely did have a slight effect on the upstream boundary layer flow, the effect was minimal. The implementation of a full propulsion system would likely have a larger effect on upstream flow and boundary layer re-energization.

Overall, airframe propulsion integration and the implementation of a BLI system present a complex and challenging design optimization problem. Aircraft engines are sized for takeoff, with the operating cruise point being a percentage of full throttle. By introducing BLI, it may be possible to scale down the size of the engines, thus reducing wetted area (and overall drag) and aircraft weight, which would increase the benefit of BLI at a system level even further. However, the addition of a BLI system will likely add weight to the aircraft, which will then require more overall thrust at take-off and additional lift at cruise. If the BLI system does not produce at least that much additional thrust, the size of the wing mounted engines, as well as the wing area, would need to be increased, further increasing weight and cost. Also, keeping the engine sized the same for take-off but throttling down to a lower operating cruise point may cause the propulsive efficiency to decrease and specific fuel consumption to increase; however, the total mission fuel would likely decrease. In addition, at a lower operating cruise point, harmful environmental emissions should decrease due to lower combustor temperature and overall pressure ratio of the engine.

A recent investigation by Welstead and Felder [33] into BLI from an overall design and propulsion architecture standpoint, as opposed to the aerodynamic, CFD perspective used in this work, examined some of the potential issues with BLI outlined above. Their work evaluated a turboelectric commercial transport architecture with two underwing turbofan engines and a rear fuselage, axisymmetric, boundary-layer ingesting fan. Results from this study indicate that the addition of BLI would actually allow for the reduction of underwing engine wetted area, along with overall aircraft weight, as well as a fuel burn reduction of 7 to 12 percent, thus invalidating some of the potential issues of BLI highlighted previously. Another recent investigation by Lv et al. [34] into the performance of conceptual BLI and wake ingestion systems suggests that a design criterion based on the potential net benefit should be considered.

The purpose of this work is not to declare whether or not BLI should be implemented in the real world, but instead serve as a starting point for designing and evaluating the potential benefit of a BLI system in this application. This analysis shows that implementing an ideal BLI system in the above fashion can provide a significant benefit in terms of propulsive power reduction and therefore, warrants further, more detailed study. As mentioned earlier, a more realistic design exercise must include the interaction of the BLI system with induced drag. Likewise, this analysis does not take into account systemic losses that would be dependent on actual engine design and implementation. In addition, this work does not look into the structural effects that implementing a BLI system might have. Ideally, the entire system, including required thrust, wing area, aircraft weight, and engine design variables would be ‘clean sheet’ designed to meet the desired design goals.

References

[1] Smith, A. M. O. and Roberts, H., “The Jet Airplane Utilizing Boundary-layer Air for Propulsion,” *Journal of the Aeronautical Sciences (Institute of the Aeronautical Sciences)*, Vol. 14, 1947, pp. 97–109.

[2] Douglass, W., “Propulsive Efficiency with Boundary-Layer Ingestion,” McDonnell Douglas, Tech. Rep. MDC J0860, August 1970.

[3] F. R. Goldschmied, “On the Aerodynamic Optimization of Mini-RPV and Small GA Aircraft,” AIAA-1984-2163, August, 1984.

[4] Roepke, J. "An Experimental Investigation of a Goldschmied Propulsor;" MS Thesis, California Polytechnic State University, 2012.

[5] Daggett, David L., Ron Kawai, and Doug Friedman. "Blended Wing Body Systems Studies: Boundary-Layer Ingestion Inlets with Active Flow Control," *NASA CR*-212670, 2003.

[6] Uranga, A., Drela, M., Greitzer, E., Titchener, N., Lieu, M., Siu, N., Huang, A., Gatlin, G. M., and Hannon, J., “Preliminary Experimental Assessment of the Boundary-Layer Ingestion Benefit for the D8 Aircraft”, AIAA-2014-0906 Oct. 2014.

[7] Pandya, S. A., Uranga, A., Espitia, A., and Huang, A., “Computational Assessment of the Boundary-layer Ingesting Nacelle Design of the D8 Aircraft,” AIAA-2014-0907, Oct. 2014.

[8] Sabo, K. M., and Drela, M., “Benefits of Boundary-Layer Ingestion Propulsion, ” AIAA-2015-1667, Mar. 2015.

[9] Berrier, B., and Allan, B., “Experimental and Computational Evaluation of Flush-Mounted, S-Duct Inlets,” AIAA-2004-764, May 2004.

[10] Rodriguez, D., “A Multidisciplinary Optimization Method for Designing Boundary-layer Ingesting Inlets,” *Journal of Aircraft,* Vol. 46, No. 3, 2009, pp. 883-894.

[11] Smith, L. H., “Wake Ingestion Propulsion Benefit,” *Journal of Propulsion and Power*, Vol. 9, No. 1, 1993, pp. 74–82.

[12] Arntz, A., Atinault, O., Destarac, D., and Merlen, A., “Exergy-based Aircraft Aeropropulsive Performance Assessment: CFD Application to Boundary-Layer Ingestion,” AIAA-2014-2573, June 2014.

[13] Plas, A., Crichton, D., Sargeant, M., Hynes, T., Greitzer, E., Hall, C., and Madani, V., “Performance of a Boundary-layer Ingesting (BLI) Propulsion System,” AIAA-2007-450, Aug. 2007.

[14] Anderson, J. D., *Fundamentals of Aerodynamics*, 3rd ed. McGraw-Hill, Boston, 2001, pp. 68-75.

[15] Lv, P., Rao, A. G., “Conceptual Analysis of Boundary-Layer Ingestion Towards Aircraft Propulsion Integration,” ISBAE-2013-1436, June 2013,

[16] Küchemann, D., and Johanna W., *Aerodynamics of propulsion*. Vol. 2. McGraw-Hill, Boston, 1953, pp. 205-209.

[17] Blumenthal, B., “Computational Investigation of a Boundary-Layer Ingestion Propulsion System for the Common Research Model.”, MS Thesis, The Pennsylvania State University, University Park, PA, May, 2016.

[18] Vassberg, J., Dehaan, M., Rivers, M., and Wahls, R., “Development of a Common Research Model for Applied CFD Validation Studies,” AIAA-2008-6919, June, 2008.

[19] Yamamoto, K., Tanaka, K., and Murayama, M., “Comparison Study of Drag Prediction for the 4th CFD Drag Prediction Workshop using Structured and Unstructured Mesh Methods,” AIAA-2010-4222, June, 2010.

[20] Turner, M. G., Reed, J. A., Ryder, R., and Veres, J. P., “Multi-Fidelity Simulation of a Turbofan Engine With Results Zoomed Into Mini-Maps for a Zero-D Cycle Simulation,” Vol. 2, Turbo Expo, 2004, 2004.

[21] "TetrUSS: USM3D Overview." *TetrUSS: USM3Dns Online Manual*. NASA Langley Research Center, 8 Aug. 2003. Web. 1 Feb. 2016. <http://tetruss.larc.nasa.gov/usm3d/overview.html>.

[22] Jones, S., NASA GRC Reference model for 90000 lb thrust class direct-drive turbofan, 2011.

[23] Drela, M., “Power Balance in Aerodynamic Flows,” AIAA Journal Vol. 47, No.7 pp.1761-1771, June, 2009.

[24] Pirzadeh, S., “Progress Toward a User-Oriented Unstructured Viscous Grid Generator,” AIAA-1996-0031, Jan. 1996.

[25] Lytle, J. K. "The Numerical Propulsion System Simulation: An Overview." *NASA CR*-209915, 2000.

[26] "Basic NPSS Gas Turbine Engine Modeling." Wolverine Ventures, 10 June 2010. Web. 13 Jan. 2015. <http://www.wolverine-ventures.com/images/pdf/basic_npss.pdf>.

[27] Kirby, M., Barros, P., and Mavris, D., "Enhancing the Environmental Policy Making Process with the FAA's EDS Analysis Tool," AIAA-2009-1262, May 2009.

[28] Campbell, R., "Efficient Viscous Design of Realistic Aircraft Configurations," AIAA-1998-2539, June 1998.

[29] Morrison, J., "Statistical Analysis of CFD Solutions from the Fourth AIAA Drag Prediction Workshop," AIAA-2010-4673, June 2010.

[30] Levy, D., Laflin, K., Vassberg, J., Tinoco, E., Mani, M., Rider, B., Brodersen, O., Crippa, S., Rumsey, C., Wahls, R., Morrison, J., Mavriplis, D., and Murayama, M., "Summary of Data from the Fifth AIAA CFD Drag Prediction Workshop," AIAA-2013-0046, May 2013.

[31] Rivers, M., and Hunter, C., "Support System Effects on the NASA Common Research Model," AIAA-2012-0707, Sep. 2012.

[32] Blumenthal, B., Elmiligui, A., Geiselhart, K., Campbell, R., Maughmer, M., and Schmitz, S., "Computational Investigation of a Boundary-Layer Ingestion Propulsion System for the Common Research Model." AIAA-2016-3812, June 2016.

[33] Welstead, J., and Felder, J., "Conceptual Design of a Single-Aisle Turboelectric Commercial Transport with Fuselage Boundary Layer Ingestion," AIAA-2016-1027, Jan. 2016.

[34] Lv, Peijian., Rao, A., Ragni, D., Veldhuis, L., "Performance Analysis of Wake and Boundary-Layer Ingestion for Aircraft Design," *Journal of Aircraft*, Vol. 1, No. 1, 2016, pp. 1–10.